Proceedings of ICAPP 2014
Charlotte, USA, April 6-9, 2014
Paper 14230

ANALYSIS AND APPLICATIONS OF A GENERALIZED MULTI-FIELD TWO-FLUID APPROACH FOR TREATMENT OF MULTI-SCALE INTERFACIAL STRUCTURES IN HIGH VOID-FRACTION REGIMES

Gustavo Montoya[1, 2], Dirk Lucas[1], Eckhard Krepper[1], Susann Hänsch[1], Emilio Baglietto[2]

[1]*Computational Fluid Dynamics Department*
Institute of Fluid Dynamics
Helmholtz-Zentrum Dresden-Rossendorf,
P.O Box 51 01 19, 01314 Dresden, Germany
g.montoya-zabala@hzdr.de

[2]*Nuclear Science and Engineering Department*
Massachusetts Institute of Technology
77 Massachusetts Avenue, Cambridge
MA 02139-4307
gmontoya@mit.edu

Abstract – *This paper presents the application of a recently developed concept for the treatment of multiphase flows, where different scales in terms of interfacial structures can be found. This approach, known as Generalized TwO Phase flow or GENTOP, considers the definition of a fully-resolved continuous gas phase where the continuous gas summarizes all gas structures which are large enough to be resolved within the computed mesh. The concept works as part of an extension of the bubble population balance approach known as the inhomogeneous MUltiple SIze Group (MUSIG), which allows the consideration of different bubble size groups, each with its own velocity field inside the dispersed phase. Within the polydispersed gas, bubble coalescence and breakup allow the transfer between different size structures, while the modeling of mass transfer between the polydispersed and continuous gas, allows considering transitions between different gas morphologies depending on the flow situations. Within the concept, different parametric studies have been made for co-current vertical gas-water pipe flow, and comparisons against experimental data for all the current calculations are shown. The experiments have been conducted in the TOPFLOW and the MT-Loop facilities at the Helmholtz-Zentrum Dresden-Rossendorf. It was shown that to consider a concept for treatment of high void fraction regimes multiphase flow as a multi-scale problem by fully resolving large, deformable, and semi-continuous gaseous structures, when considering the right physics behind the phenomena, it is able to reproduce the flow behavior from experimental data both, in a quantitative and qualitative way.*

I. INTRODUCTION

In nuclear power plants, Computational Fluid Dynamics (CFD) codes have been increasingly gaining importance during the last years. This is especially true in case of safety analysis of accident scenarios, where accurate and predictive calculations are needed in order to understand and avoid those circumstances. One example of such cases can be found within the KERENA reactor, a European concept of boiling water reactor (BWR), where instabilities have been reported to occur due to flashing boiling and high gas volume fractions in one of its passive safety systems known as GEKO or Gebäudekondensator[1].

As in the KERENA case, most of the safety research analysis within the nuclear industry require predictive simulations of the thermal hydraulics of steam-water multiphase flow systems. While for several years, CFD codes have been widely developed and validated mainly for single phase flow, the prior applications in the nuclear science, as well as in many others fields such as in chemical engineering or medicine, has been attracting researchers to improve numerical methods in the multiphase flow area. Since the complexity of the interface increases with higher void fraction regimes, most of the advancements in modeling multiphase flows has been focus for a long time in the accurate prediction of bubbly flows, which is not sufficient to satisfy the current industry needs.

The boiling phenomenon, for example, is composed by a series of flow regimes and subsequent transitions, such as bubbly flow, slug or churn-turbulent regime, and annular flow. In order to fully understand and predict these phenomenon, the higher void fraction regimes must be also

CASL-U-2014-0072-000

taken into account. Churn-turbulent, for example, is characterized by high gas volume fractions (in excess of about 30%) and represents one of the most convoluted flow pattern that can be found in gas-liquid two-phase flow systems. The churn-flow can be observed in large pipes when high superficial gas velocity and low superficial liquid velocity are used. While for small diameter pipes and similar flow conditions, the slug regime can be observed where the characteristic Taylor bubble rises in the system follow by a number of smaller bubbles entrained in its tail. Both regimes are characterized by a mixture of large and small interfacial scales.

In terms of CFD, the Eulerian multi-fluid approach is widely used to describe dispersed flows patterns such as bubbly or droplet flows, since such regimes are characterized by scales of interfacial structures which are smaller than the grid size. For flow situations with large-scale interface like film-, annular or horizontal stratified flows, usually interface tracking methods are used. In principle, the interface capturing methods should be utilized for interfacial length scales several times larger than the grid size, while for an averaged two-fluid approach, bubble sizes smaller than the grid size are required[2]. While relatively successful calculations have been made in the past for high void fraction regimes using the Eulerian averaging approach[3], many challenges have been reported due to the difficulties of establishing closure laws that can successfully represent the physics behind the highly deformable large bubbles encountered in these regimes.

Since in the case of such high void fraction flows, dispersed gas structures, and large interfaces occur simultaneously, a combination of these modeling concepts would be needed (Fig. 1). While Tomiyama[4] addressed the open questions regarding the gap in the scales for intermediate range of interfacial structures, combinations of these two basic computational techniques has been proposed since many years ago, for example by Černe[5], who explicitly coupled a VOF-method and an interface capturing algorithm with the Eulerian two-fluid model using a switch criterion based on the error of the VOF-method depending on the dispersion of the interface, but they were not able to predict transition from dispersed to stratified flow. Tomiyama and Shimada[6] proposed a hybrid method using a level-set approach for capturing the interface along with a multi-fluid method, but did not consider bubble breakup and coalescence. Minato[7] proposed an extended two-fluid model, where large scales were treated with a VOF-method differencing scheme, and later on Strubelj[8] combined the two-fluid model with a conservative level set method. Within their concept, the interface sharpening method as well as a surface tension model[9] were validated, but no transitions between small- and large scale gas phases were considered.

A novel concept based on a two-phase four-field modeling technique with continuous and dispersed gas, which also consider phase transfer between different gas morphologies as well as bubble coalescence and breakup has been developed, and validated qualitatively against well-known cases such as dam-break[10], impinging jet, and bubble-columns. This paper will present further developments of the concept based on different parametric studies, qualitative comparison of pipe flow cases, as well as the first numerical validation of the concept based on the experiments of the TOPFLOW and MT Loop facilities at the Helmholtz-Zentrum Dresden-Rossendorf. The simulations for parametric studies and validations have been made using the CFD code CFX 14.5.

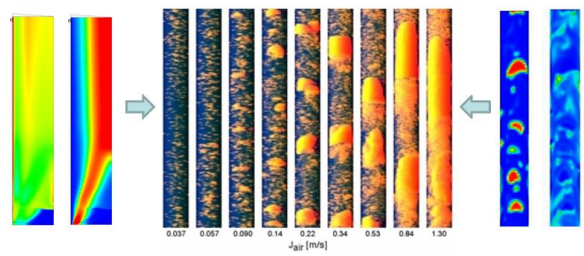

Fig. 1. Exemplification of the modeling of different interfacial scales using an Eulerian averaging multi-fluid approach[3] and the GENTOP concept on churn-turbulent flow regime.

II. COMPUTATIONAL FLUID DYNAMICS (CFD) MODEL FORMULATION

A two-phase multi-field CFD approach was created to simulate a two-phase co-current vertical pipe flow. This multi-field modeling concept is based, in principle, on ensemble averaging the respective governing equations for each component fluid. When using this modeling approach with adequate closure laws, this method should be able to accurately represent the dispersed gas-field from the current calculations.

The resulting conservation equations, which are commonly used, are shown in (1) and (2), and represent the mass and momentum conservation equations respectively.

$$\frac{\partial(\alpha_k \rho_k)}{\partial t} + \nabla \cdot (\rho_k \alpha_k \mathbf{v}_k) = m_k''' \tag{1}$$

$$\frac{\partial(\alpha_k \rho_k \mathbf{v}_k)}{\partial t} + \nabla \cdot (\rho_k \alpha_k \mathbf{v}_k \mathbf{v}_k) = -\alpha_k \nabla \mathrm{p}_k + \nabla \cdot \left(\alpha_k \underline{\underline{\tau}}_k\right) + \rho_k \alpha_k \mathbf{g} + \sum_{\boldsymbol{j}} \mathbf{M}_{kj}^{i} + \sum_{\boldsymbol{m}} m_{m,k}''' \mathbf{v}_{\boldsymbol{m}}^{\boldsymbol{i}} \tag{2}$$

Where $m_k''' = \sum_m m_{m,k}'''$

In the aforementioned equations, α_k represents the volume fraction of the field-k, while $m'''_{m,k}$ is the volumetric mass transfer term from other fields which represents the same phase into field-k. The term $\underline{\underline{\tau}}_k = \underline{\underline{\tau}}_k{}^{\mu} + \underline{\underline{\tau}}_k{}^{Re} = \mu_k(\nabla \mathbf{v}_k + \nabla \mathbf{v}_k{}^{\boldsymbol{T}}) - \frac{2}{3}\mu_k \nabla \cdot \mathbf{v}_k \boldsymbol{I}$ is the total shear stress term.

The variable $\mathbf{M}^i_{kj}$ represents the interfacial momentum transfer per unit time between two different fields.

II.A. Polydispersed Modeling: Description of the Mechanistic Models for Interfacial Forces

One of the key aspects when modeling using an Euler-Euler averaging approach is the correct consideration of closure laws in order to obtain a good representation of the hydrodynamic behavior on multiphase flows. The objective behind the formulation of closure laws is to reintroduce some of the information which is lost by the averaging of the conservation equations by accounting for the mass and momentum transfer between the different fields and phases while providing the functional form which is expected for the interfacial forces.

The different forces acting at the interface of the flow are divided into drag and non-drag components. The interfacial non-drag forces taken into account for the modeling of the dispersed phase in this work are the lift force, the wall force, and the turbulent dispersion force.

$$\mathbf{M}^i_k = \mathbf{M}^D_k + \mathbf{M}^{ND}_k \tag{3}$$

$$\mathbf{M}^i_k = \mathbf{M}^D_k + \mathbf{M}^{TD}_k + \mathbf{M}^L_k + \mathbf{M}^W_k \tag{4}$$

The drag contribution model use in this research work is given as

$$\mathbf{M}^D_{d,k} = \frac{3}{4}\alpha_{d,k}\frac{\rho_c}{d_b}C_{D,k}\left|\mathbf{v}_c - \mathbf{v}_{d,k}\right|\left(\mathbf{v}_c - \mathbf{v}_{d,k}\right) \tag{5}$$

The drag coefficient has been calculated as proposed by Ishii and Zuber[11]. The following equations represents the correlation for the drag coefficient for spherical cap, ellipse, and distorted bubbles respectively.

$$C_{D,k\,(cap)} = \frac{8}{3}(1-\alpha_k)^2$$

$$C_{D,k\,(ellipse)} = \frac{2}{3}Eo^{\frac{1}{2}} \tag{6}$$

$$C_{D,k\,(distorted)} = \min(C_{D,k\,(ellipse)}, C_{D,k\,(cap)})$$

In terms of non-drag forces, the turbulent volume fraction dispersion force known as Favre averaged drag force, as proposed by Burns[12], is included with the objective of taking into account the increased in mixing due to turbulence in the multiphase flow. The turbulent dispersion transport the dispersed gas phase in a direction opposing the void fraction gradient.

$$\boldsymbol{M}^{TD}_{\boldsymbol{c}} = -\boldsymbol{M}^{TD}_{\boldsymbol{c}} = C_{TD}C_{cd}\frac{\nu_{tc}}{\sigma_{tc}}\left(\frac{\nabla\alpha_d}{\alpha_d} - \frac{\nabla\alpha_c}{\alpha_c}\right) \tag{7}$$

Here the C_{cd} term represents the interface drag force coefficient. The term σ_{tc} refers to the turbulent Schmidt number for the continuous phase volume fraction.

The interfacial lift force has been implemented in order to account for the momentum exchange due to lift between the continuous and dispersed phases.

$$\boldsymbol{M}^L_{d,k} = -C_L\rho_c\alpha_{d,k}(\mathbf{v}_{d,k} - \mathbf{v}_c) \times (\nabla \times \mathbf{v}_c) \tag{8}$$

The lift coefficient (C_L) has been calculated as proposed by Tomiyama[13].

$$C_{L,k} = \min\left(0.288\,tanh(0.121Re_k), f(Eo_k)\right)\ for\ \ Eo_k < 4$$

$$C_{L,k} = f(Eo_k)\ for\ \ Eo_k < 4 \tag{9}$$

$$C_{L,k} = -0.27\ for\ \ Eo_k > 10$$

Where $f(Eo_k)$ is defined as shown in equation (10). It is known that the critical bubble diameter at which the lift force change sign can be found by solving the roots of this correlation which gives a value of 5.8 mm under atmospheric pressure and room temperature for air bubbles in water[14].

$$f(Eo_k) = 0.00105{Eo_k}^3 - 0.0159{Eo_k}^2 - 0.0204Eo_k + 0.474 \tag{10}$$

In order to account for the hydrodynamic force acting on a bubble which moves in a close proximity to a wall, the interfacial wall force has been used as proposed by Tomiyama[14].

$$\boldsymbol{M_{d,k}}^{\boldsymbol{W}} = -C_W\frac{d_b\alpha}{2}\left(\frac{1}{y^2}\right)\rho_c w^2_{rel}\overrightarrow{n_r} \tag{11}$$

The wall coefficient (C_W) used in this work has been implemented as proposed by Hosokawa[15] which is valid for high and low Morton numbers provided that the bubble does not collide with the wall.

$$C_W = \max\left\{\frac{7}{{Re_k}^{1.9}}, 0.0217Eo_k\right\} \tag{12}$$

Finally, the turbulent effect induced by the bubbles on the continuous liquid phase has been taken into account by implementation of two additional source terms describing

the bubble effects for *k* and *w*-equations proposed by Rzehak and Krepper[16].

II.B. The GENTOP -concept

A GEneralized TwO Phase flow (GENTOP) –concept has been recently developed, and it will be validated in the present work against vertical pipe flows in high void fraction regimes using three-field two-fluid simulations. At the moment, GENTOP consist of a continuous liquid phase l, a polydispersed gas phase dg, and a continuous gas phase cg.

II.B.1 The Inhomogeneous MUSIG approach

A bubble population balance approach known as Inhomogeneous MUltiple SIze Group (MUSIG) proposed by Krepper et al. (2005), has been used for the small-scale dispersed gas phase. This allows the dependency of the momentum exchange on the bubble sizes having a great influence on the drag and non-drag forces[14, 17]. The MUSIG concept allows a division of the dispersed phase into a number of N velocity groups (or phases), where each velocity group is characterized by its own velocity field. Then, the overall bubble size distribution is further represented by dividing the bubble diameter range within each of the velocity groups j into a number, M_j (j = 1 … N), bubble size fractions (Fig. 2). Furthermore, this population balance model considers bubble coalesce and breakup into the sub-size groups, which means that the mass exchange between the sub-size groups can also exceed the size ranges assigned to the velocity clusters[18].

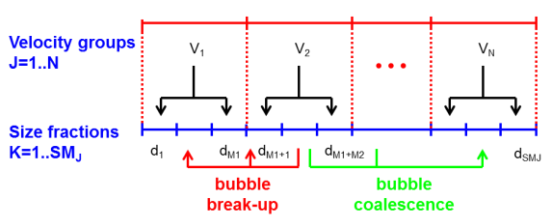

Fig. 2. Improvement of the polydispersed approach: the size fractions M_j are assigned to the velocity field V_j

The GENTOP –concept has been developed in principle as an extension of the inhomogeneous MUSIG approach by adding a continuous gas phase. The mass transfer between dispersed and continuous gas is modelled depending on the flow situation, and as a first step to demonstrate the principle, the last velocity group included within the MUSIG framework is considered as the new continuous gas (Fig. 3). Later on, more advance transition models between the dispersed and continuous gas, different from breakup and coalescence inside the dispersed gas fractions via MUSIG definition, have to be developed. This velocity group represents all gas structures which are larger to an equivalent spherical bubble limit diameter $d_{dg,max}$. In the past[2] the threshold diameter $d_{dg,max}$ has been considered grid dependent since it was expected that a complete resolution of the gas-liquid interface occurs only if the continuous gas structure contain several grid cells. A maximum diameter of $d_{dg,max} = z\Delta x$ was chosen, where z = 4 is based on the knowledge of the smearing of the interface in between 2-3 cells when using the Eulerian approach. During this work, it will be shown that z = 2.3, and even z = 1 are acceptable values to obtain a very good representation of the physical behavior behind the continuous gas. There is an on-going work to further study the grid-dependency and in order to avoid such behavior in the future by improving the resolution of the continuous gas using other methods as it will be explained later in this paper.

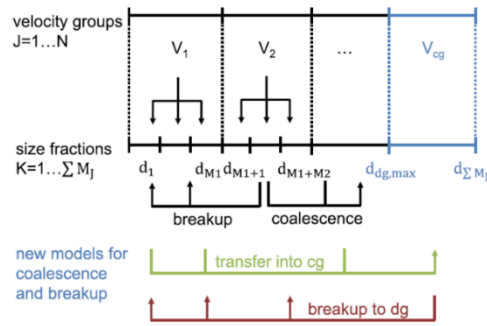

Fig. 3. Schema of the extended inhomogeneous MUSIG-model including a continuous gas phase.

II.B.2 Tracking of the Interface

In order to be able to resolve the gas structures within the GENTOP concept, the first step is to localize the interface. An appropriate blending function φ_{fs} is used in order to identify the local interfacial structure. Due to the averaged treatment of the Euler-Euler approach, the expected volume fraction discontinuity at the interface, has been replaced by a gradient of volume fraction. For that reason, a free surface region is defined using the volume fraction gradient of the continuous gas $|\nabla\alpha_{cg}|$. The interface between the gas and the liquid is characterized by a variation of the volume fraction of $\nabla\alpha_{cg}$ from 0 to 1 over a number of n grid cells of a Δx size, which leads to a critical value $|\nabla\alpha_{cg}|_{crit} = 1/(n\Delta x)$ that allows a definition of the interface (Fig. 4). The free surface function is defined as

$$\varphi_{fs} = 0.5\tanh\left[a_{fs}\Delta x\left(|\nabla\alpha_{cg}| - |\nabla\alpha_{cg}|_{crit}\right)\right] + 0.5 \qquad (13)$$

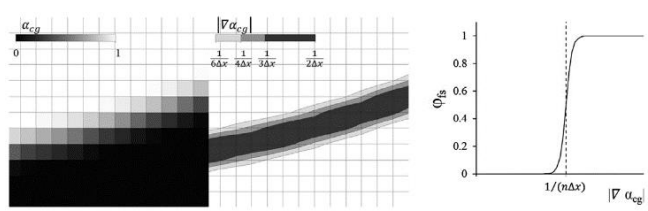

Fig. 4. Detail of a continuous gas-liquid interface, and blending function for a filtered interface[2] (a_{fs}=100).

II.B.3 Clustering-method

A clustering force has to be defined, in order to consider transitions from the dispersed towards the continuous gas phase using an aggregative effect within the volume fraction of the continuous gas. As expected, modeling using an Eulerian two-fluid approach will produce smearing of volume fraction by numerical diffusion. This method also counteracts that behavior producing interface stabilizing effects.

The clustering influence has been defined as an additional interfacial force acting exclusively between the continuous gas and liquid phases and it is included within the interfacial momentum transfer as it can be observed in equation (14). In past publications[2, 10] a mistake was made by stating this force acts contrary to the gradient of the volume fraction of the liquid. In reality the force acts proportional to this gradient of volume fraction, as it is shown in equations (14) and (15).

$$\overrightarrow{\mathbf{M}_j} = \overrightarrow{\mathbf{M}}_{j,D} + \overrightarrow{\mathbf{M}}_{j,clust} \tag{14}$$

Where,

$$\mathbf{M}_l{}^{clust} = \mathbf{M}_{cg}{}^{clust} = c_{clust}(1-\varphi_{fs})\varphi_{clust}\rho_l\nabla\alpha_l \tag{15}$$

At the moment in which a specific critical void fraction of the continuous gas is reached, and the assumption of averaged treatment of the dispersed phase is no longer valid, the force will create regions of continuous gas volume fraction by inducting aggregation on the continuous gas phase volume fraction until a complete formation of gas structures is reached (Fig. 5).

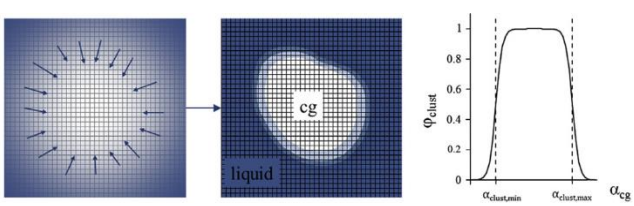

Fig. 5. Schema of cluster-effect on newly formed continuous gaseous void fraction, and blending function method of clustering[2] ($a_B = 20$)

This force not only allows an observable transition from dispersed into continuous gas with the appearance of a filtered interfaces between the gas and the liquid, but also if the volume fraction gradient decreases near a free surface region due to numerical diffusion, the force counteracts the liquid gradient of volume fraction, and reduces the smearing effect.

The constant defined as c_{clust} regulates the intensity with which the force acts within the fluid domain depending on the flow situation. In the present cases, since a strong formation of continuous structure due to an intense coalescence effect is expected, the maximum value of 1.0 has been used. The fact that such an important force depends only on the gradient of volume fraction of the liquid is not an optimal condition, as it will be shown in the results part of this research work. Further studies are needed in order to produce a more physical-dependent definition of this clustering method.

The blending function φ_{clust} acts inside the computational domain as shown in Fig. 5, and is defined as

$$\varphi_{clust} = \left(0.5\tanh\left[a_B\left(\alpha_{cg} - \alpha_{clust,min}\right)\right] + 0.5\right) \cdot \left(0.5\,x\tanh\left[a_B\left(\alpha_{clust,max} - \alpha_{cg}\right)\right] + 0.5\right) \tag{16}$$

II.B.4 Interfacial Transfers

In order to define an accurate interfacial transfer model depending on the corresponding amount of volume fraction presented, transitions between dispersed and continuous gas must be considered. This can be achieved by detecting the local gaseous morphology and by using a similar idea as that of the AIAD-model[20], defining a corresponding switch between the closure models by introducing new formulations for the interfacial area density A_D and drag coefficient C_D in order to consider free surfaces for the interfacial transfer of mass and momentum (Fig. 6).

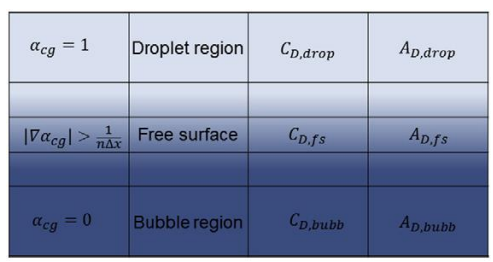

Fig. 6. Volume fractions and corresponding morphologies where the droplet and free surface regions correspond to the continuous formulations of A_D and C_D.

The switch between morphologies has been set to an $\alpha_{cg,crit} = 0.3$, based on the knowledge that bubbly flow rarely exceeds a void fraction between 0.25 and 0.35 when a transition to resolved structures occurs[21, 22, 23]. Based on a blending function φ_{morph}, the formulations for interfacial area density and drag are defined as

$$\varphi_{morph} = 0.5\tanh\left[a_B\left(\alpha_{cg} - \alpha_{cg,crit}\right)\right] + 0.5 \tag{17}$$

$$C_{D,cg} = \left(1-\varphi_{morph}\right)C_{D,bubb} + \varphi_{morph}C_{D,cont} \tag{18}$$

$$A_{D,cg} = \left(1-\varphi_{morph}\right)A_{D,bubb} + \varphi_{morph}A_{D,cont} \tag{19}$$

In order to allow the occurrence of droplets inside the continuous phase, a free surface and a droplet region were defined within the continuous morphology.

$$C_{D,cont} = max\left[\varphi_{fs} C_{D,fs}, (1-\varphi_{fs}) C_{D,drop}\right] \tag{20}$$

$$A_{D,cont} = max\left[A_{D,fas}, A_{D,cont}\right] \tag{21}$$

Three different drag coefficients are being applied, $C_{D,bubb}$ for the bubbly regions where $\alpha_{cg,crit}$ has not been reached, $C_{D,fs}$ where a free surface is detected by the free surface function, and $C_{D,drop}$ for the droplet regions formed within the continuous gas structures. For the bubble region, a drag formulation as proposed by Ishii and Zuber and explained in the prior section was used. For the droplet region, the drag coefficient is assumed constant and equal to 0.44, while for the free surface region, where the drag is ruled by skin friction which is caused by viscous surface shear stresses, a formulation proposed by Höhne and Vallee[24] has been used.

$$C_{D,fs} = max\left[0.01, \frac{2\left[\alpha_l \tau_{w,l} + \alpha_{cg} \tau_{w,cg}\right]}{\rho_l u^2{}_{slip}}\right] \tag{22}$$

For cases such as the one presented in this research work, where very large and deformable bubbles are formed, a special treatment for the turbulence at the free surface must include sub-grid information which depends on the grid resolution. The consideration of sub-grid turbulence effect within the free surface has been already implemented within the GENTOP -concept following the work of Broccini and Peregrine (2001), but it has not been considered for the cases presented in the current work.

Similar to the drag formulations, the interfacial area density is applied as three different equations. In terms of the bubble and droplet regions, the area density is based on particle model formulations, while for the free surface region it depends of both, continuous gas and liquid. In the presented cases, the volume fraction of the liquid was set to a minimum value α_l =1e-07 inside the continuous phase, since no droplets are being considered.

$$A_{D,bubb} = \frac{6\alpha_{cg}}{d_{cg}} \tag{23}$$

$$A_{D,fs} = \frac{\left(2|\nabla\alpha_l|\left|\nabla\alpha_{cg}\right|\right)}{\left(|\nabla\alpha_l| + \left|\nabla\alpha_{cg}\right|\right)} \tag{24}$$

$$A_{D,drop} = \frac{6\alpha_l}{d_l} \tag{25}$$

Finally, in order to account for the lift effect on bubbles which are larger than the pre-established limit bubble diameter based on the last MUSIG group but still have not reached a continuous morphology ($\alpha_{cg,crit} < 0.3$), a lift coefficient formulation has been introduced as follows

$$C_L = \left(1 - \varphi_{morph}\right) \cdot (-0.27) \tag{26}$$

Which should be set to zero at the moment in which the dispersed gas within the secondary gaseous phase reached a continuous morphology.

II.B.5 Complete Coalescence

A special coalescence method for complete gaseous mass transfer has been established within the concept in order to replace the coalescence due to the averaged coalescence models when the pre-defined critical void fraction $\alpha_{cg,crit} = 0.3$ is reached. At that point, the coalescence rate increases sharply, turning all the remained dispersed gas, within a specific grid cell, into continuous gas. The idea behind this mechanism is to enforce the fact that small bubbles cannot occupy the same space where a large quantity of continuous gas is located. The complete coalescence method has been turned off inside the free surface, in order to allow coalescence and breakup at those positions. The mass transfer is defined as

$$\dot{m}_{dg\to cg} = \left(1 - \varphi_{fs}\right) \cdot \varphi_{morph} \cdot \rho_{dg} \cdot \alpha_{dg} \cdot \frac{1}{\tau_{dg\to cg}} \tag{27}$$

Where $\tau_{dg\to cg} = 20\Delta t$ represents a time constant that regulates how fast the mechanism occurs in consistency with the numerical scheme.

An illustration which exemplifies how the GENTOP concept works, can be observed in Fig. 7.

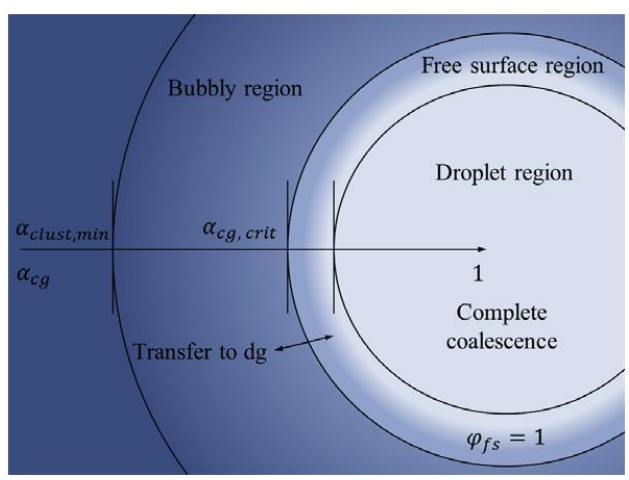

Fig. 7. The GENTOP –concept and its principles[2].

II.C. Coalescence and Breakup for the Polydispersed and the Continuous Gas-Phases

For the definition of both, the polydispersed and continuous gas phases within the calculations presented in this work, it has been assumed that seven groups of bubbles of different diameters enter the flow channel. These bubbles will eventually start to coalesce, creating a large spectrum of new structures larger than the original bubbles. The opposite process will also occur making the large bubbles breakup into smaller ones.

The coalescence mechanism is modeled as proposed by Prince and Blanch[25] taking into account the collision frequency of the bubbles and the efficiency of collision based on the film drainage model. Breakup mechanism are related to the impact of turbulent eddies on bubble surfaces using the model developed by Luo and Svendsen[26] which is based on the theory of isotropic turbulence. In that model, the occurrence of breakage is determined by the energy of arriving eddies which can participate in the bubble's deformation and breakup, only if they are of a size smaller than or equal to the bubble diameter. Intensity rates are added to the mass transfer rates in these models to harmonize the calculated results with experimental data. These are set as dimensionless factors F_C for coalescence and F_B for breakup. In the present calculation only the breakup coefficient has been lowered to 0.5, due to the high over prediction of breakup rates as discussed by Krepper[27].

For future calculations, the breakup and coalescence models proposed by Liao[28], which has been created in order to consider different mechanisms for breakup and coalescence within the MUSIG framework, will be implemented and validated within GENTOP. The interactions that this concept considers for coalescence are due to turbulence laminar shear, wake-entrainment, and eddy capture. For bubble breakup Liao's model considers the effect due to turbulent fluctuation, laminar shear, and interfacial slip velocity.

III. DESCRIPTION OF THE EXPERIMENTAL FACILITIES

The simulations presented in this research paper, have been validated using an experimental database for air-water two-phase flows in vertical stainless steel pipes with diameters of 51.2 mm and 195.3 mm, that has been extracted from the thermal-hydraulic test facilities TOPFLOW (Fig. 8) and MT-Loop (Fig.9) at the Helmholtz-Zentrum Dresden-Rossendorf. These databases provide information about the evolution of the two-phase flow along the pipe height. In order to achieve this, several measurements with varying distances between the gas injection and the measurement plane were made for different combinations of gas and water flow rates. The pressure at the gas injection is kept constant at 0.25 MPa. Ensuring this, the measured data represents the evolution along the pipe as if the gas injection was in a fixed position and the measurement plane varies.

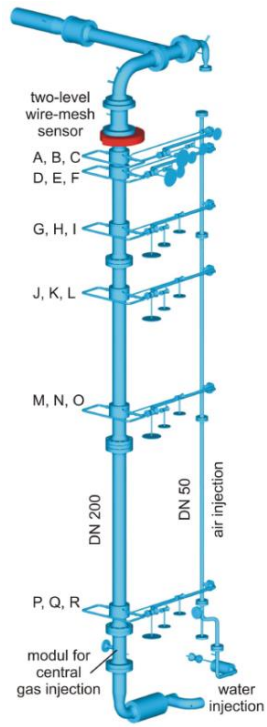

Fig. 8. Vertical test section of the TOPFLOW facility with variable gas injection system.

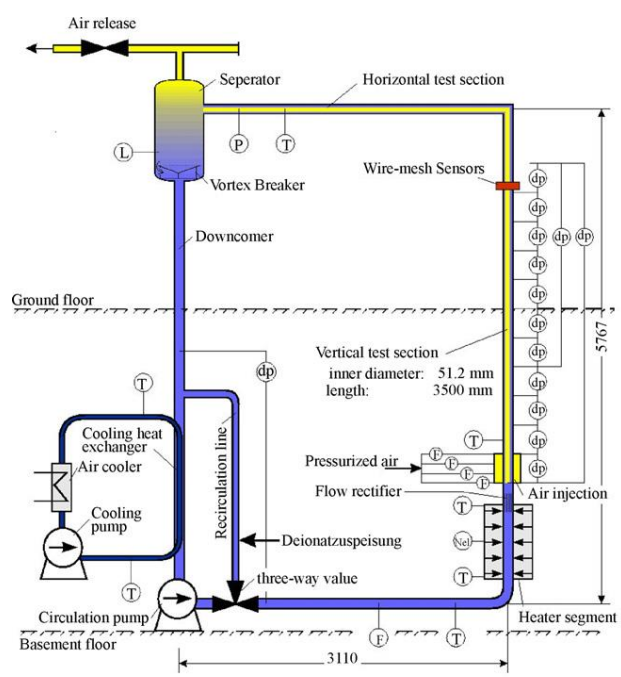

MT-Loop

Fig. 9. MT-Loop experimental facility.

The test section at the TOPFLOW facility is equipped with six gas inlet locations which allowed the injection of air or steam via orifices in the pipe wall, while the MT Loop experimental facility counts with an equally distributed sparger injection also with different distance to the measurement plane. The liquid phase was supplied also from the bottom of the test section. Both facilities count with a measurement plane that consists in a two-level wire-mesh sensor. The lower sensor is used for obtaining data regarding the gas volume fraction profiles and bubble size distributions, while the second one is utilized to determined gas velocities by cross-correlation of both sensors. The results of these experiments are the time averaged radial profiles of the gas fraction, the gas velocity, the time and cross-section averaged bubble sized distributions, and the fraction data regarding the resolved bubble sized and spatial distribution.

IV. COMPUTATIONAL GRID AND BOUNDARY CONDITIONS

Two cases from the TOPFLOW and MT-Loop experimental studies were taken for the validation of the presented model as it can be observed from table 1. Case 129 is under churn-turbulent flow conditions, while case 118 is considered to be a transitional flow from bubbly to churn-turbulent regime.

The data corresponding to the inlet conditions at the liquid continuous phase in the multiphase modeling (turbulent kinetic energy, and turbulent eddy dissipation) were taken from fully developed single phase simulations calculated on the same computational grid, while the velocity profile is calculated from the TOPFLOW experiments. The inlet boundary conditions for the gas phase have been taken from the experimental data given by TOPFLOW at L/D = 1.1 and by MT-Loop at L/D = 0.6, including gas velocity, mass flow rate, and size fractions.

TABLE I
Initial conditions used in the simulations

Run number	Superficial liquid velocity (m/s)	Superficial gas velocity (m/s)
118	1.017	0.219
129	1.017	0.342

On the present simulations using the GENTOP –concept, the experimental data regarding the gas phase was arrange into two velocity groups. The first group contains size fractions up to 5.8 mm, while the second group represents bubbles larger than the prior mentioned size. The limit in the bubble sizes in order to establish the difference between one gas-field and the other, is given by the change on the sign of the Tomiyama lift force.

The simulations are based to replicate the experimental conditions established in both, the TOPFLOW and MT-Loop air-water flow in a vertical test section experiments (Fig. 10). Five meshes were used for the calculations shown in these research work. The first one is an axisymmetric 40 x 800 grid with refined cell size of 1.5 mm near the wall, and 0.5 mm near the inlet with the same dimension as the TOPFLOW facility. The second and third one are semi-2D channels, one with symmetry condition at half-diameter. The second one has a mesh size of 15 x 1150 and a homogenous cell size of 7 mm, and the third one has a mesh size of 29 x 1150, and also a cell size of 7 mm. The last mesh is a full 3D geometry. It is based on the MT-Loop facility, and have a cell size of 3 mm. The meshing software utilized were ANSYS ICEM CFD, ANSYS Design Modeler, and ANSYS Mesh.

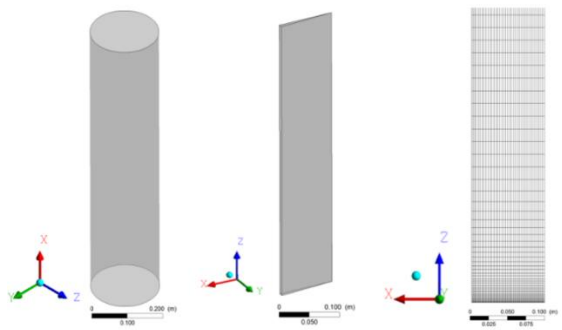

Fig. 10. 3D and 2D axisymmetric pipe geometries, and 2D axisymmetric mesh with unequal nodal distribution[3].

V. RESULTS AND DISCUSSIONS

Extensive testing has been performed on the proposed modeling approach using the experimental conditions corresponding to various data series from TOPFLOW and MT-Loop experiments with the objective of validating the GENTOP –concept under high void fraction conditions.

The first aim of this research work was to produce comparative simulations of those presented by Montoya[2] using TOPFLOW L12 case 129 experimental conditions, in which a full Euler-Euler multi-fluid averaging approach was used along with a series of closure laws, in order to study the advantages of fully resolving the continuous gas-phase instead of trying to model the physical behavior with approximated closure laws. To keep the computational efforts within reasonable limits, an axisymmetric 2D geometry was used along with an equivalent mesh as the one from the prior mentioned contribution. Two planes of symmetry were defined at the upper and lower sides of the mesh and one at the correspondent axis, in order to establish a condition in which the gradient of the fluid properties (e.g., void fraction and velocities) are equal to zero (Fig. 11).

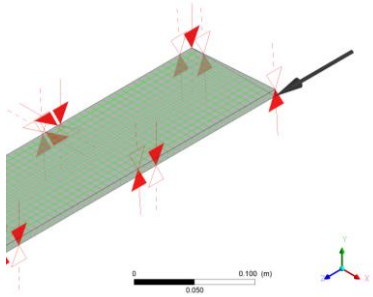

Fig. 11. Illustration of the used 2D-Axisymmetric mesh with specified symmetry conditions (red arrows) and inlet boundary (black arrow).

At this first attempt, the concept within the calculation was able to produce an apparently-satisfactory resolution of the continuous gas, as it can be observed at the left side of Fig. 12. Here, when reaching the outlet of the axisymmetric domain, it clearly shown a fully resolved first slug-type bubble, along with the corresponding entrained dispersed gas in its tail at t = 2.1 seconds. At the moment in which the continuous gas reached the axis of the domain, a further calculation of the continuous morphology is not possible, introducing a strong and sudden mass transfer of all the continuous gas into the dispersed morphology, producing a complete destabilization of the calculation.

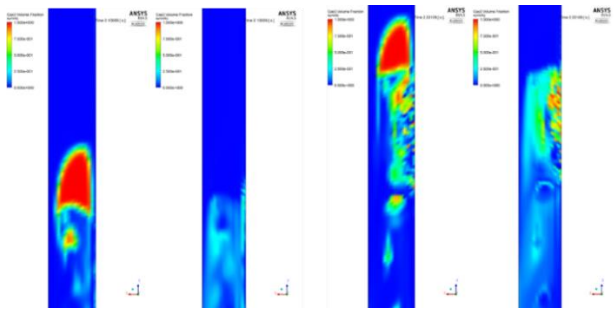

Fig. 12. Left: Behavior of the continuous and dispersed phases before reaching the axisymmetric 4º angle, right: Unphysical flow behavior when trying to resolved the continuous gas at the axis symmetry boundary.

The continuous slug-like gas structure is completely destabilized when reaching the axis of the domain due to the inability to keep resolving the continuous morphology within the 4º of aperture cells at the axisymmetric boundary. While it is common to try to reduce the computational time of numerical simulations by using less complex meshes, in general, the assumption of a cylindrical axisymmetric simplification in the computation, prevents lateral motion of the gas phase and leads to an unrealistic void fraction distribution wherein a maximum volume fraction of the gas is away from the centerline. Also, there are significant instantaneous radial and azimuthal liquid velocity components which cannot be captured in a 2D axisymmetric simulation[29].

The next step was to produce a general analysis of the symmetry conditions when using the GENTOP approach in order to prove that the inability of resolving the continuous gas in the prior mentioned study was due to the grid cells at the axis side, and not to the symmetry plane itself. For this study, also the conditions from the case 129 from the TOPFLOW experimental facility were used. For the first calculation, a mesh of a semi-2D channel was used with homogeneous cell size of 7 mm, symmetry conditions in the upper and lower planes and at the center of the domain for one of the calculation, and with a full radial domain in the other simulation (Fig.13).

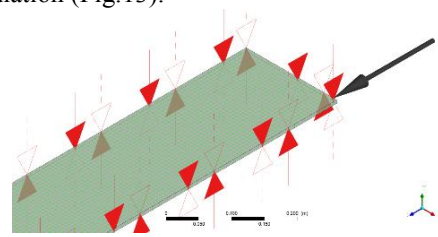

Fig. 13. Illustration of the used semi-2D channel-like mesh with specified boundary and symmetry conditions.

The calculation which is characterized by a symmetry condition at the center of the radial domain, was not destabilized by the symmetry plane, allowing to conclude that the effect observed in the prior calculation was due to the resolution on the axisymmetric cells morphology rather than the symmetry plane itself. When qualitatively studying the void fraction distribution across the pipe (Fig. 14), it can be observed that the continuous gas begin to appear rather late in the pipe, and during at least half of the domain, there is a high quantity of continuous gas that remains unresolved. This behavior is maintained until almost three quarter of the pipe. Furthermore, it appears that in this regions when getting closer to the symmetry condition, the numerical diffusion is higher, probably destabilizing the proper formation of the interface. For the last part of the pipe, churn-like fully resolved deformable bubbles can be observed, followed by the expected entrainment of dispersed gas.

Two interesting observations that can be noticed already are regarding the behavior of the free surface when getting closer to both, the wall and symmetry boundary conditions. It can be observed, that when the interface of a fully resolved bubble reaches the wall boundary condition, the void fraction of the continuous gas at the wall cell can be as high as one. The reason for this, is the lack of a surface tension formulation within the free surface, basically leaving the resolved bubble with nothing that can pushed them away from the wall. This is a behavior that repeats in other cases to be shown in this research paper, and an implementation of a surface tension model within the free surface is being though to be implemented in the GENTOP model in the future in order to avoid that effect. This result will be further discussed later on with the 3D simulations.

While the behavior of the continuous gas close to the wall is quite logical, in the moment that this secondary gas reached the symmetry condition, the void fraction within the interface of the resolved structure does not change, impeding the continuous gas to "merge" with the symmetry boundary, and for that matter, producing an overprediction of the void fraction at that specific location in time.

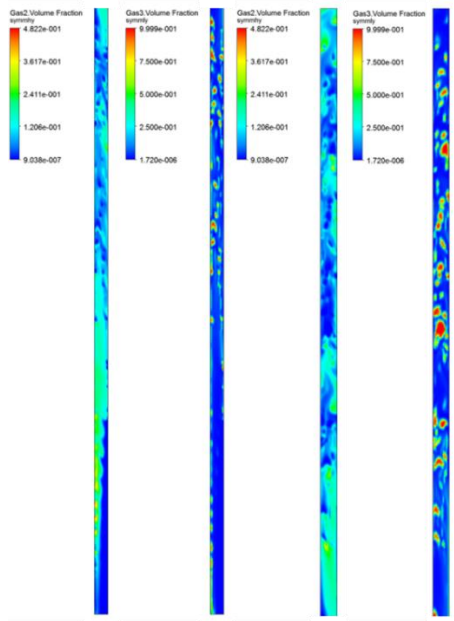

Fig. 14. Distributions of void fraction for dispersed and continuous gas phases for the first (left) and second (right) half of the pipe consider half of the radial domain.

For the next case, in which no symmetry plane is considered, the appearance of continuous structures occurs much sooner in the domain, triggered by small continuous bubbles merging sooner within the pipe, a behavior which is not possible when considering the symmetry plane (Fig. 15).

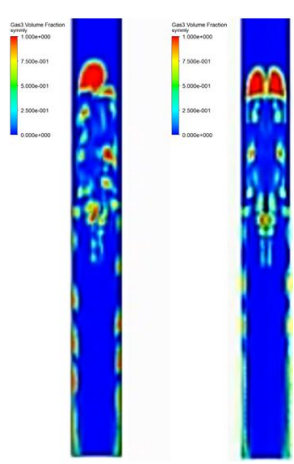

Fig. 15. Behavior of continuous morphologies close to the injection plane with and without symmetry, respectively.

When observing qualitatively the distribution of the void fraction when no symmetry conditions are considered, the behavior early in the pipe and for the evolution of the flow until higher positions is significantly different as observed when symmetry conditions are used. Basically, as explained before, the formation of the continuous gas occurred since early in the pipe, and leads to a much higher void fraction of the continuous gaseous phase. Another behavior which can be observed in the calculations that consider no-symmetry conditions, is the appearance of flow entrainment forming vortex-like structures regarding the dispersed gaseous phase after the formation of the first continuous structures, behavior that cannot be replicated when considering a symmetry plane (Fig. 16).

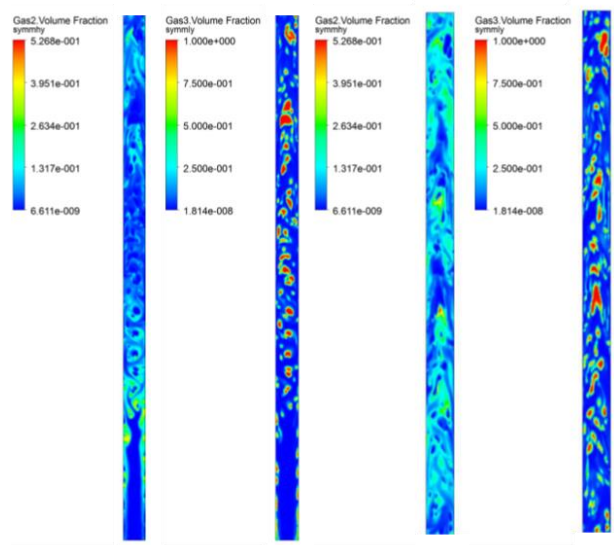

Fig. 16. Distributions of void fraction for dispersed and continuous gas phases for the first (left) and second (right) half of the pipe considering the full radial domain.

Therefore, future GENTOP simulations should take into account complete 3D fully transient environments in order to be able to predict the different flow behavior and aforementioned characteristics of the continuous morphology. Due to the limitations in terms of computational resources when preparing calculations with large dimensional grids such as in the case of the DN 200 vertical pipe from the TOPFLOW facility, a decision has been made to use the MT Loop experimental data. This facility while having different gas injection conditions, works with similar flow behavior and fluid velocities within a smaller dimensional grid, allowing faster and more resource efficiency calculation for experimental validations and comparison.

The next calculations were established as full-set 3D models of the MT-Loop facility using the experimental conditions of case 118 in a relatively-homogenous mesh

with a 3 mm cell size (Fig. 17). The convergence criteria established for the simulations was based on a RMS of 1E-4, with 4 minimum coefficient (inner iteration) loops and 30 maximum loops. All of the calculation took around 5 to 8 loops for the internal iteration step to convergence.

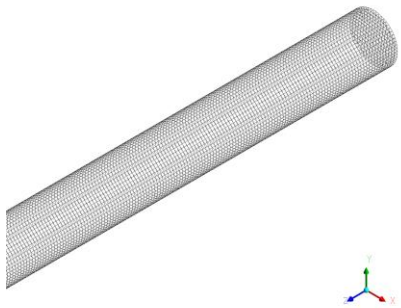

Fig. 17. Illustration of 3D homogeneous mesh used for the MT-Loop calculations considering a 3 mm cell size.

A qualitative view of the calculation, allow to observe a very different behavior than that of the TOPFLOW simulations (Fig. 18). In this case, for the first half of the axial domain, instead of obtaining a relatively quick dispersion of the inlet gas injection from the sparger, it increases the void fraction at the center of the pipe as a possible effect from the clustering force, acting too strongly in the direction of the gradient of liquid volume fraction, and for that matter, pushing too strongly the continuous gas towards the center of the domain. This behavior was not observed when the gas was injected from the wall of the pipe.

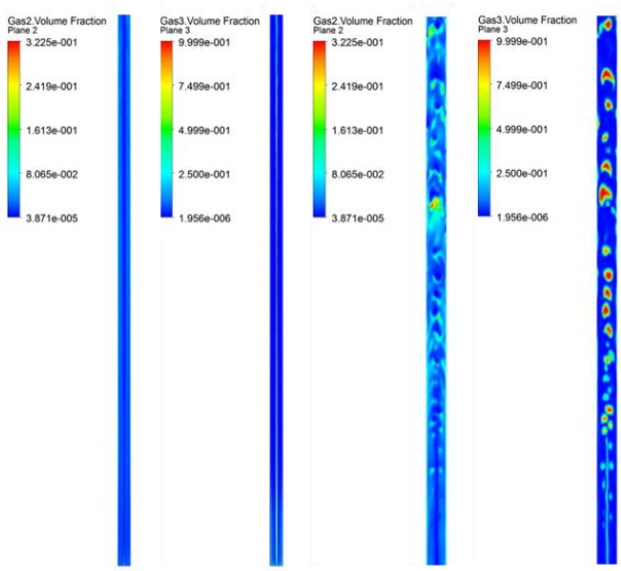

Fig. 18. Plane contour representation of an MT-Loop simulation based on case 118 using the GENTOP –concept.

When comparing against the experimental data for quantitative analysis, a good prediction in terms of the bubble size distribution for the polydispersed gaseous phase can be observed (Fig. 19).

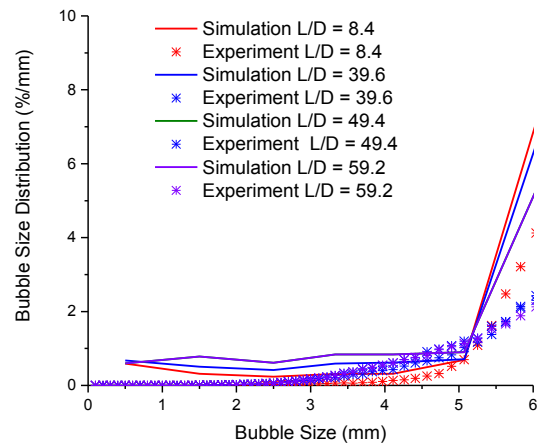

Fig. 19. Validation of dispersed gas bubble size distribution against the MT-Loop experimental data case 118.

In terms of radial void fraction, the strong peaks observed before in the qualitative analysis for almost half of the pipe, can also be seen in the quantitative comparison (Fig. 20). While in the experiments, the total void fraction is almost completely dispersed by an L/D = 8.4, it is not until an L/D = 39.6 that the total void fraction in this simulation began to disperse obtaining a good agreement by L/D = 49.4, and a very good result when comparing against the highest measurement plane at L/D = 59.2. In terms of averaged and individual gas velocities, the agreement against experiments is always very good, showing the small peaks, as expected, where the maximum of higher bubble sizes (Gas3) are, and improving when increasing the height in the domain (Fig. 21).

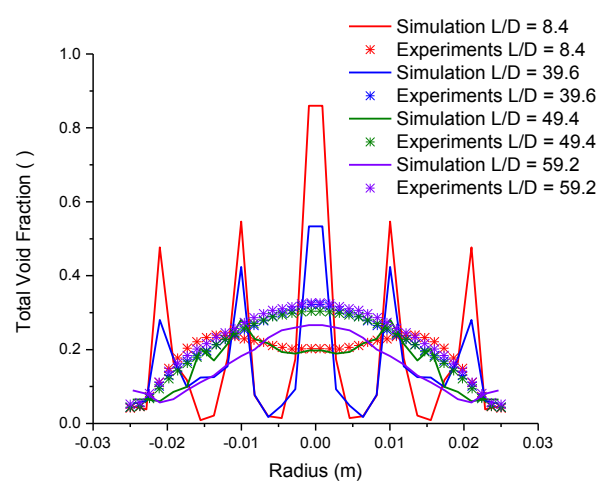

Fig. 20. Validation of the radial total void fraction against the MT-Loop experimental data case 118.

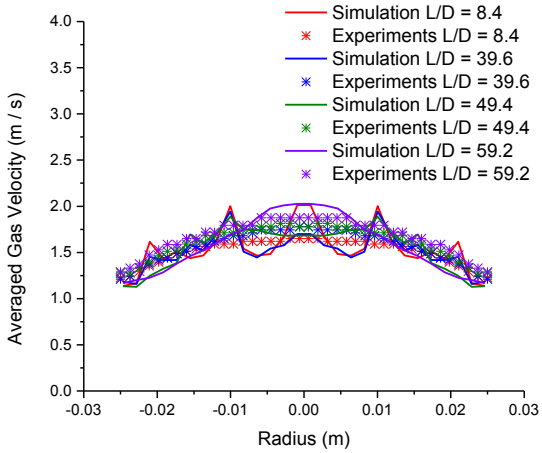

Fig. 21. Validation of the gas averaged velocity against the MT-Loop experimental data case 118.

Another reason for the long stripes observable in the simulations, could be due to the idealized conditions in the URANS models, and so the problem is expected to vanish if large eddies would be resolved. A different approach for a temporal solution could be to solve the calculation by superposing the gas inlet with some periodicity conserving the time averaged flow rate. The dependency of the bubble size on the frequency of such a periodic or chaotic perturbation is being investigated. Also the time dependent cross section averaged void fraction from the measurements can be taken to have a perturbation of the inlet conditions. For this work, it was thought that a possible solution could have been to consider lowering the coefficient within C_{td} which, as it was explained before, allow to control the intensity of the clustering force. A test case was considered, lowering this coefficient from 1.0 to a value of 0.1 (Fig. 22). As it can be seen, there is nearly no change in the overall profile in terms of the lack of void fraction radial dispersion, having a decrease at the center of the domain of only 4E-2.

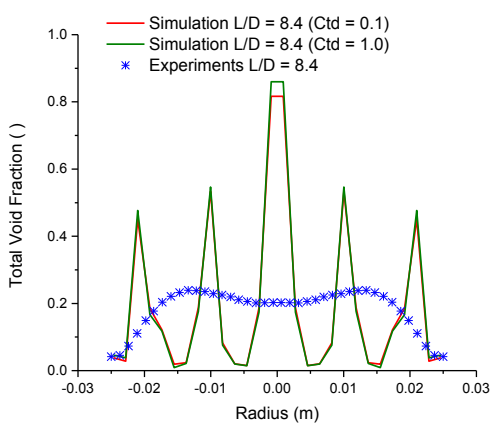

Fig. 22. Validation of the radial total void fraction considering a C_{td} = 0.1 and C_{td} = 1.0.

In terms of the clustering force, the dependability of the inverse of the liquid volume fraction is an obvious setback for the concept. At this time, behavior of bubbles cluster are being intensively study in order to establish a more physical relation between the clustering method and the behavior of the flow, in order to avoid problems as the ones mentioned before.

It was observed in prior implementations of the concept, as for example in bubble column cases that the continuous structures after being resolute, used to lower their velocity, and then increase it again. After a complete check of the implementation, it was found that in the complete coalescence model, a misconception of the momentum of the continuous phase was made, in which after the complete coalescence was activated, the dispersed gas that remained in the cell was transformed into continuous gas, transferring all the mass from dispersed to continuous morphology, but the velocity was set to zero.

This defined velocity produced an unphysical behavior within the continuous structures in the domain. This deviation was corrected by considering a velocity equal to the dispersed gas local velocity, being able now to conserve momentum. This is a behavior which is easier to observed into a qualitatively frame per frame analysis, than in a time averaged velocity comparison. As an exemplification, a slightly faster slug for the same time value can be observed in Fig. 23 in a 3D iso-volume representation of the flow for the same case based in void fraction of continuous structures ($0.3 < \alpha_{cg} < 1.0$).

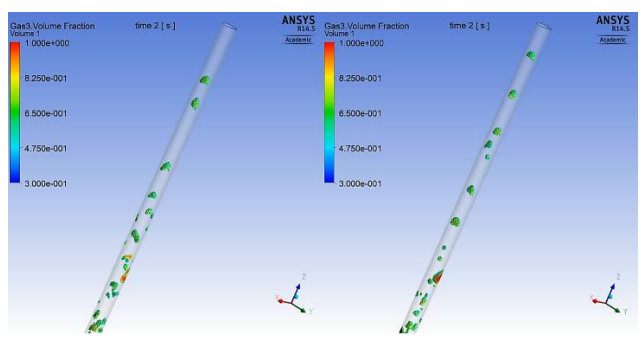

Fig. 23. Iso-volume representation of $0.3 < \alpha_{cg} < 1.0$ without (left) and with (right) correct implementation of the complete coalescence method.

Another important effect that can be observed, as mentioned before, in all the studied cases is the increased of void fraction near to the wall of the pipe (Fig. 24). It can be observed that in every calculation, when a bubble get close the wall, the interface disappears, and the gaseous continuous structure get a void fraction close or equal to unity. This occurs, as explained before, because there is a lack of surface tension at the free surface, and so there is

nothing to push the bubble away from the wall, once that goes in contact with the wall boundary. While this effect can only be observed as a small peak close to the wall side when study the radial void fraction of higher measurement levels (Fig. 25), this could also be producing an under-prediction of void fraction at the centerline of the pipe in time, since the bubble is, in theory, not expected to move during a long time at the side of the boundary wall layer.

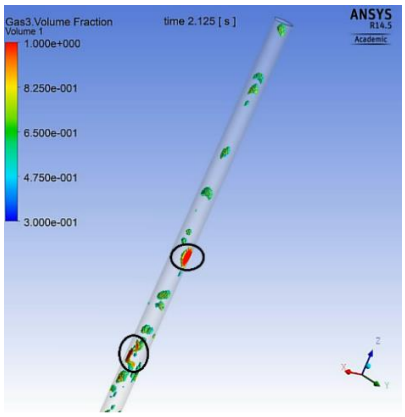

Fig. 24. Iso-volume representation of an MT-Loop calculation case 118 where a void fraction equal to unity can be found at the wall boundary layer.

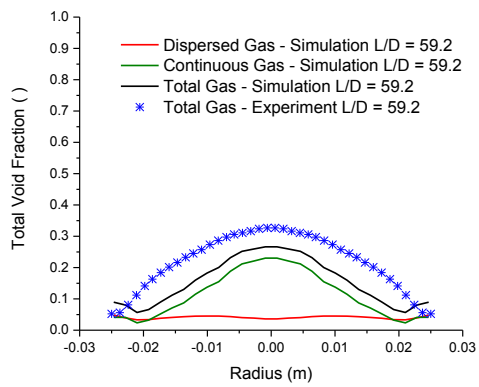

Fig. 25. Void fraction radial distribution of MT-Loop calculation case 118 where the overprediction of void fraction is observable at the wall side.

Another assumed condition in prior calculations, is that of a free-slip boundary condition for all gaseous phases. This assumption allows the gas to move freely at the wall cells without lowering its velocity. While this condition is applicable for the polydispersed gas, at the moment in which the secondary gas phase becomes a continuous structure, then the condition should not applied anymore, since as a continuous fluid, a wall friction effect is supposed to occur, lowering the corresponding velocity of the continuous structure close to the wall. For that matter, a no-slip boundary condition has been established for the continuous gas. In order to study the effects of this change, the radial velocity profile for the continuous gaseous phase, for the total gas phase, and the radial profile for the void fraction are shown (Fig. 26, Fig. 27, and 28). In those cases, only the last two measurement levels are shown, not taken into account the "transitional zone" prior mentioned in the discussion.

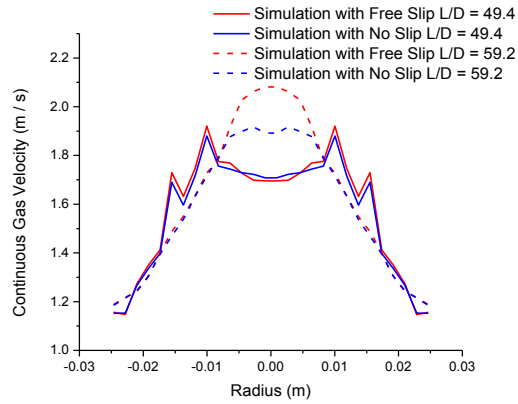

Fig. 26. Velocity radial profile comparison of the last two measurement levels for the continuous gas.

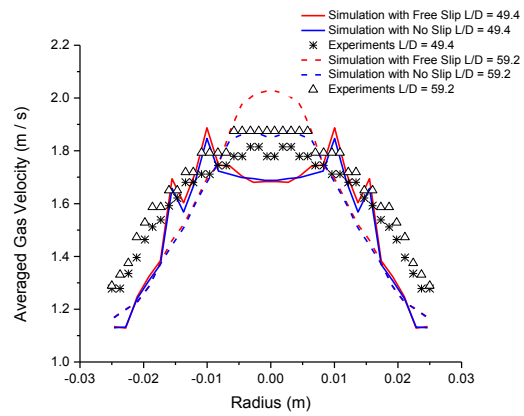

Fig. 27. Averaged gas velocity radial profile comparison of the last two measurement levels for 118 MT-Loop case.

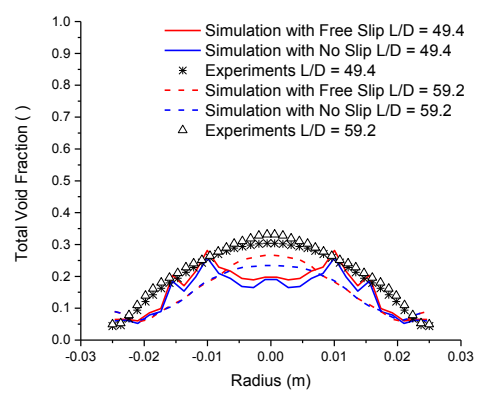

Fig. 28. Total void fraction radial profile comparison of the last two measurement levels for 118 MT-Loop case.

As it can be observe from the figures, the effect of considering a non-slip boundary condition, affects the whole radial profile diminishing the values of velocity for the continuous gas, especially when getting closer to the center of the domain. As expected, since the continuous gas represents the higher void fraction within the domain, it dominates the velocity within the pipe, and so the values of velocity with or without considering the dispersed gas are almost equal. Furthermore, the effect of the non-slip boundary condition, not only affects the radial profile of the gas velocity, but it also has an effect in the volume fraction radial distribution of the gas, slightly reducing the total void fraction at the center of the pipe.

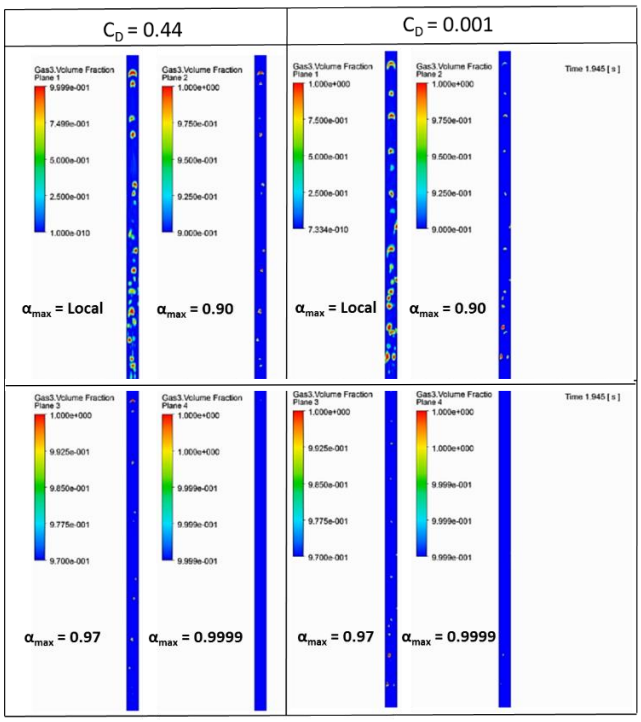

Fig. 29. Plane contour representation of the continuous gas for study of bubble resolution.

Finally, another important subject to discuss is regarding the resolution of the continuous structures. Theoretically, it is assumed that a continuous bubble is completely resolved when it contains a non-trivial number of cells within its domain where the void fraction is equal to, at least, 0.9999. This resolution has been proven difficult to achieve since the beginning of the concept. Commonly, apparently-resolved bubbles contains values of void fraction of around 0.9700 to 0.9900. While with this values, the apparently-resolved structures have been able to reproduce the behavior of the flow, especially for higher measurement planes in pipe flows, in a very accurate manner, the problem needs to be address and solve, in order to improve the morphology, and for that matter the behavior of the continuous gas. A possible solution would be to consider a fourth field in order to fully model the possible dispersed liquids or drops forming inside the continuous gas. Since that is not a trivial task, an intermediate step in order to improve the resolution of the bubbles, could be to lower the drag coefficient for the drops in order to make the liquid within the continuous gas to fall towards the liquid wall-film of the bubbles. Two calculations were made in order to consider a parametric study, where the drag coefficient of the drops is lower from its original value of 0.44, to 0.22 and 0.001. While in both cases, the apparent resolution of gas considering a void fraction for the continuous gas acceptable as 0.97, 0.99, and 0.9999, seems to improve (Fig. 29), the refinement is rather insignificant for the destabilization effect that lowering this drag coefficient produce in the overall calculation. A possible solution to this problem, to be implemented in the near future, would be to consider the clustering force to blend out within the free surface, but not inside the continuous gas.

VI. CONCLUSIONS

The presented work has shown the achievement of a series of important objectives in the studies of high void fraction regimes when treated as a multi-scale problem. These results give, significant insights in the analysis of boiling related-situations and accident scenarios in nuclear safety research.

The results have shown that a multi-scale approach to multiphase simulations, where large deformable gas structures are explicitly resolved on the base of physical subgrid models, has the potential to reproduce the experimentally observed flow behavior both in a quantitative and qualitative way..

The proposed concept has shown particularly good predictions for the fully developed flow region of the experimental setup, while shortcomings are still observed during the flow development. The evidenced limitations have been discussed in this work, and preliminary solutions have been proposed and are being assessed. It has also been noticed that the specific challenges observed in the first half of the pipe (transition zone), are related to the specific sparger injection in the small pipe tests, which did not produce a uniformed distribution. This is not expected to occur in the larger TOPFLOW vertical test section. Complete 3D numerical comparison are being performed for this case to verify this conclusion. At the same time the physical approach behind the clustering method within the presented concept is also being updated in order to produce a more general implementation.

Finally, useful conclusions have been derived on the grid sensitivity method. While previous work[2] had suggested a switch between morphologies for bubble sizes 4 times the cell length ($D_B = 4\Delta x$), it has been shown in this

paper that the concept has sufficient grid independency, and that considering a $D_B = 2.3\Delta x$, and even $D_B = \Delta x$, allow acceptable resolution of the flow, with accurate predictions of radial profiles at an L/D = 59.2. This finding indicated that the GENTOP concept might be applicable to relatively low computational resource analyses for fast industrial scale turnaround times.

VII. ACKNOWLEDGMENTS

This work is carried out in the framework of an on-going research project funded by E.ON Kernkraft GmbH, and in cooperation with the Nuclear Science and Engineering Department of the Massachusetts Institute of Technology (MIT).

VIII. NOMENCLATURE

Notation

C_D Drag coefficient.
C_L Lift coefficient.
C_{cd} Interphase drag force coefficient for the FAD turbulence dispersion model.
C_{TD} Turbulent dispersion coefficient.
C_{VM} Virtual mass coefficient.
C_W Wall force coefficient.
C_μ Coefficient for viscosity.
d_b Bubble diameter.
Eo_k Modified Eötvos number.
g Acceleration due to gravity.
m_k''' Volumetric mass transfer term into field-k from other fields representing the same phase.
$\mathbf{M}_{kj}^i$ Interfacial momentum transfer per unit time between the fields k and j.
p Absolute pressure.
r_d Drag radius [m].
Re_k Reynolds number of the *k*-phase.
t Time [s].
$\mathbf{v}_k$ Phase-k averaged velocity.
$\mathbf{v}_m$ Mass averaged mixture velocity.
w_{rel} Relative velocity.

Greek letters

α Void fraction.
ε Turbulent eddy dissipation term.
κ Turbulent kinetic energy.
μ Viscosity.
ρ_k Density of the phase-k.
φ Blending function.
σ_{tc} Turbulent Schmidt number for the continuous phase volume fraction.
$\underline{\tau}_k$ Total shear stress term.
$\underline{\tau}_k{}^{\mu}$ Total shear stress term due to viscosity.
$\underline{\tau}_k{}^{Re}$ Total shear stress term due to the Reynolds number.
ω Turbulent frequency term.

Superscripts

i Interfacial.
D Drag.
ND Non-drag.
VM Virtual mass.
TD Turbulent dispersion.
L Lift.
W Wall.

Subscripts

c Continuous phase.
cg Continuous gaseous phase.
$clust$ Clustering.
d Dispersed phase.
j Index.
k k-phase.

IX. REFERENCES

1. Leyer, S.; Wich, M. "The Integral Test Facility Karlstein". Sci. Tech. Nucl. Inst., Article ID: 439374 (2012).

2. Hänsch, S.; Lucas, D.; Krepper, E.; Höhne, T. "A multi-field two-fluid concept for transitions between different scales of interfacial structures". Int. J. Mult. Flow 47:171-182 (2012).

3. Montoya, G.; Liao, Y.; Lucas D.; Krepper, E. "Analysis and Applications of a Two-Fluid Multi-Field Hydrodynamic Model for Churn-Turbulent Flows". Proc. 21th Int. Conf. of Nucl. Eng. ICONE21-16297, China (2013).

4. Tomiyama A.; Sakoda, K.; Hayashi, K.; Sou, A.; Shimada, N.; Hosokawa, S. "Modeling and hybrid simulation of bubbly flow". Multiphase Sci. Technol. 18 (1): 73-110 (2006).

5. Černe, G.; Petelin, S.; Tiselj, I. 'Coupling of the interface tracking and the two-fluid model for the simulation of the incompressible two-phase flow". J. Comput. Phys. 171: 776-804 (2001).

6. Tomiyama, A.; Shimada, N. "(N+2)-field modeling for bubbly flow simulation". Comput. Fluid Dyn. J. 9 (4): 418-426 (2001).

7. Minato, A.; Takamori, K.; Ishida, N. "An extended two-fluid model for interphase behavior in gas-liquid two-phase flow". Proc. 8th Int. Conf. Nucl. Eng., ICONE-8045, April 2-6, Baltimore, USA (2000).

8. Strubelj, L.; Tiselj, I.; Mavko, B. "Simulations of free surface flows with implementation of surface tension

and interface sharpening in the two-fluid model". Int. J. Heat Fluid Flow 30: 741-750 (2009).

9. Brackbill, J.U.; Kothe, D.; Zemach, C. "A continuum method for modeling surface tension". J. Comput. Phys. 100: 335-354 (1992).

10. Hänsch, S.; Lucas, D.; Höhne, T.; Krepper, E.; Montoya, G. "Application of a multi-field concept to the dam-break case with an obstacle". Proc. of the 15th International Topical Meeting on Nuclear Reactor Thermalhydraulics, NURETH-15, Pisa, Italy (2013).

11. Ishii, M.; Zuber, N. "Drag Coefficient and Relative Velocity in Bubbly, Droplet or Particle Flows". AIChE J., 25: 843-855 (1979).

12. Burns, A.; Frank, T.; Hamill, I.; Shi, J. "The Favre Averaged Drag Model for Turbulent Dispersion in Eulerian Multi-phase Flows". 5th International Conference on Multiphase Flow, ICMF04, Japan (2004).

13. Tomiyama, A.; Tamai, H.; Zun, I.; Hosokawa, S. "Transverse Migration of Single Bubbles in Simpler Shear Flows". Chem. Eng. Sci., 57: 1849-1858 (2002).

14. Tomiyama, A. "Struggle with Computational Bubble Dynamics". Proceedings International Conference on Multiphase Flow, France (1998).

15. Hosokawa, S.; Tomiyama, A.; Misaki, S.; Hamada, T. "Lateral migration of single bubbles due to the presence of wall". Proceedings of ASME Fluids Engineering Division Summer Meeting, Canada (2002).

16. Rzehak, R.; Krepper, E. "Bubble induced turbulence: Comparison of CFD models". International Symposium on Multiphase flow and Transport Phenomena. Agadir, Morocco. April 22-25 (2012).

17. Lucas, D.; Krepper, E.; Prassar, H.-M. "Use of Models for Lift, Wall and Turbulent Dispersion Forces Acting on Bubbles for Poly-Disperse Flows". Chem. Eng. Sci., 62: 4146-4157 (2007).

18. Krepper, E.; Ruyer, P.; Beyer, M.; Lucas, D.; Prasser, H.-M.; Seiler, N. "CFD simulation of polydispersed bubbly two-phase flow around an obstacle". STNI Article ID 320738 (2009).

19. Krepper, E.; Frank, Th.; Lucas, D.; Prasser, H.-M; Zwart, P.J. "The Inhomogeneous MUSIG model for the simulation of polydispersed flow". Nucl. Eng. Des., 238: 1690-1702 (2008).

20. Höhne, T.; Deendarlianto; Lucas, D. "Numerical simulations of counter-current two-phase flow experiments in a PWR hot leg model using an area density model". Int. J. Heat Fluid Flow 31 (5): 1047-1056 (2011).

21. Griffith, P.; Wallis, G.B. "Two-phase slug flow". J. Heat Transfer 83: 304-320 (1961).

22. Taitel, Y;; Bornea, D.; Dukler, A.E. "Modelling flow pattern transition for steady upward gas-liquid flow in vertical tubes". AIChE J. 26 (3): 345-354.

23. Murzyn, F.; Chanson, H. "Free surface fluctuations in hydraulic jumps: experimental observation Exp. Therm. Fluid Sci. 33: 1055-1064 (2009).

24. Höhne, T.; Valle, C. "Experiments and numerical simulations of horizontal two-phase flow regimes using an interfacial area density model". J. Comput. Multiphase Flows 2: 131-143 (2010).

25. Prince, M.J.; and Blanch, H.W. "Bubble Coalescence and Break-Up in Air-Sparged Bubble Columns". AIChE J., 36(10): 1485-1499 (1990).

26. Luo, H; Svendson, H.F. "Theoretical model for drop and bubble break-up in turbulent flows". AIChE J., 42(5): 1225-1233 (1996).

27. Krepper, E.; Lucas, D.; Prasser, H.-M. "On the modelling of bubbly flow in vertical pipes". Nucl. Eng. Des. 235: 597-611 (2005).

28. Liao, Y.; Lucas, D.; Krepper, E.; Schmidtke, M. "Development of a generalized coalescence and breakup closure for the inhomogeneous MUSIG model". Nucl. Eng. Des. 24: 1024-1033 (2011).

29. Chen, P. "Modeling the Fluid Dynamics of Bubble Column Flows". PhD Dissertation, Washington University (2004).